To be submitted to *Limnology & Oceanography Letters*

Extreme value distributions describe interannual variability in the North Atlantic spring bloom

Gregory L. Britten
Program in Atmospheres, Oceans, and Climate
Massachusetts Institute of Technology, Cambridge, MA, USA
gregleebritten@gmail.com

Scientific Significance Statement: The North Atlantic spring bloom helps fuel the marine food web, impacts fisheries recruitment, contributes to carbon export, and is predicted to change with climate warming. Understanding interannual bloom variability is thus of central oceanographic importance. This study provides a framework for quantifying interannual bloom variability via statistical extreme value theory. We characterize the spatial distribution of extreme value parameters using satellite chlorophyll observations and test whether the distribution of chlorophyll extremes has changed over time in relation to trends in background chlorophyll levels and sea surface temperature.

Abstract

The North Atlantic spring bloom depends on a confluence of environmental factors that drive transient periods of exponential phytoplankton growth and interannual variability in bloom magnitude. We analyze interannual bloom variability in the North Atlantic via extreme value theory where the Generalized Extreme Value Distribution (GEVD) is fitted spatially to annual maxima of satellite-measured surface chlorophyll. We find excellent agreement between the observed distribution of interannual bloom maxima and those predicted from the GEVD. The spatial distribution of fitted GEVD parameters closely follows basin bathymetry where the largest extremes and heaviest distribution tails are found on the continental shelves and slopes. Trend analyses suggest weak evidence for changes in GEVD parameters, despite regional trends in mean chlorophyll levels and sea surface temperature. These results provide a framework to quantify interannual bloom variability and call for further work examining how extreme blooms propagate through food webs and contribute to carbon export.

Introduction

Phytoplankton form the base of the marine food web (Falkowski et al. 2003) and play a major role in the global carbon cycle (Falkowski et al. 1998; Ito and Follows 2005). At mid and high-latitudes, the seasonality of phytoplankton is characterized by a late-winter or spring bloom where phytoplankton biomass concentrations reach an annual maximum (Behrenfeld and Boss 2014). The spring bloom is important for sustaining higher trophic levels, including species whose annual migrations are timed to coincide with the bloom (Visser et al. 2011). Blooms also contribute to carbon export and are often associated with large export pulses to depth (Briggs et al. 2011).

Several biophysical mechanisms are thought to control bloom development (Behrenfeld and Boss 2014, 2018). For example, the critical depth hypothesis predicts that bloom initiation begins with mixed layer shoaling and associated increases in mixed layer averaged light availability

(Behrenfeld and Boss 2014, 2018). The critical turbulence hypothesis (a variant of the critical depth hypothesis) focuses on light availability in the active mixing layer (Taylor and Ferrari 2011; Ferrari et al. 2015), while the dilution-recovery hypothesis predicts that blooms develop due to changes in grazing via dilution from deepening mixed layers (Evans et al. 1985; Behrenfeld 2010). Across proposed mechanisms, the population-level phenomena of blooms arise due to transient positive imbalances between growth and loss rates such that the exponential growth rate is positive, i.e.

$$\frac{dc}{dt} = (g(t) - l(t))c,$$

with $g(t) - l(t) > 0$ prior to the bloom. Days to weeks post-bloom, losses increase to match and exceed growth, most often because of increased grazer abundance supported by the elevated phytoplankton biomass (Behrenfeld and Boss 2014, 2018). The magnitude and duration of the transient exponential growth period determines the magnitude of the spring bloom biomass maximum.

The North Atlantic basin exhibits one of the largest and well-studied seasonal blooms across the global ocean. Deep winter mixing and rapid springtime re-stratification causes ideal conditions for exponential phytoplankton growth, with bloom timing following a northward progression as re-stratification occurs earliest at low latitude (Dutkiewicz et al. 2001; Siegel et al. 2002). Meteorological variability then modulates the precise timing and magnitude of the bloom according to the impacts on local mixing dynamics (Dutkiewicz et al. 2001; Follows and Dutkiewicz 2002). Importantly, variability in bloom timing and magnitude has been linked to the magnitude of carbon export (Briggs et al. 2011) and to fisheries productivity via the 'match-mismatch hypothesis' (Platt et al. 2003). Climate change is expected to alter North Atlantic bloom dynamics via a range of factors, including changes in seasonal mixing depths, nutrient fluxes, and the metabolic impacts of warmer temperatures (Sommer and Lengfellner 2008). Quantifying the dynamics of the North Atlantic spring bloom is thus of central importance for understanding the relevant oceanographic and ecological processes and will aid in tracking the associated impacts of climate change.

Viewing interannual blooms as extreme values in observed phytoplankton time series brings to bear the statistical theory of extreme values. Under the Fisher-Tippet-Gnedenko theorem, the maximum of a sequences of random variables converges in distribution to the Generalized Extreme Value Distribution (GEVD), itself a generalization of the Gumbel, Frechet, and Weibull distributions (Coles 2001). The theorem yields a three-parameter probability density function describing the limiting distribution of maximum values generated from samples of a stochastic process, analogous to the central limit theorem for a the mean of a distribution (Coles 2001; described below). While the GEVD is increasingly applied to geophysical and climate studies (Easterling et al. 2000; Katz 2010; Aghakouchak et al. 2020). there have been fewer applications to biological time series (Batt et al. 2017). Consistent with the exponential nature of biological growth, Batt et al. (2017) found that biological time series exhibited consistently heavier tails in their extreme value distributions relative to chemical and geophysical time series. These findings suggest the North Atlantic bloom as an ideal target of extreme value analysis, due to its annually repeating cycle of transient and variable exponential growth.

Here we analyzed the North Atlantic satellite chlorophyll record to quantify seasonal phytoplankton bloom variability via extreme value analysis. We estimated GEVD parameters at a ¼° latitude-longitude scale. We mapped the fitted parameters spatially and evaluated the GEVD goodness-of-fit to the chlorophyll time series. We correlated the fitted parameters to bathymetric properties of the North Atlantic basin. We further evaluated evidence for non-stationarity (i.e., time-variability) in GEVD parameters in the context of satellite-observed chlorophyll and temperature trends across the basin. Results of this study will provide a statistical framework to describe interannual bloom variability and allow us to test an important hypothesis with respect to basin-scale environmental change.

Methods

Observations

We analyzed two sets of basin-scale satellite chlorophyll observations. First, we used chlorophyll estimates from the Moderate-resolution Imaging Spectroradiometer-Aqua (MODIS-Aqua) sensor, spanning years 2002-2021, accessed from the Oregon State University Ocean Productivity database (https://sites.science.oregonstate.edu/ocean.productivity/). Associated inherent optical properties were estimated using the Garver-Siegel-Maritorena (GSM) algorithm (Maritorena and Siegel 2005). MODIS-Aqua based chlorophyll estimates were gap-filled for missing observations due to clouds according to the algorithm described at http://orca.science.oregonstate.edu/gap_fill.php. While gap-filling can alter the underlying chlorophyll distribution, it is not expected to affect the annually measured maximum value. Secondly, we used the Ocean Colour Climate Change Initiative (OC-CCI) chlorophyll product (Sathyendranath et al. 2019) covering the same time period as the MODIS-Aqua dataset. OC-CCI chlorophyll is a synthetic product generated by combining information from multiple sensors, including SeaWiFS (Sea-viewing Wide-Field-of-view Sensor), MODIS-Aqua, MERIS (Medium spectral Resolution Imaging Spectrometer) and VIIRS (Visible and Infrared Imaging Radiometer Suite). OC-CCI was not gap-filled and therefore contained missing values due to clouds. We grided both sets of chlorophyll observations to ¼° latitude-longitude rectilinear resolution. Wintertime satellite chlorophyll observations were not available for higher latitudes due to light limitation and were replaced with a value of zero concentration which did not affect the extreme value analysis. Sea surface temperature data from the MODIS-Aqua sensor were taken from the Oregon State University Ocean Productivity Database site cited above.

Extreme Value Analysis

Given a time series of chlorophyll observations at an individual location, we estimated the parameters of the GEVD via the block maxima approach (Gilleland and Katz 2016), taking time series blocks as individual years. We define $x = \max(y_1, y_2, \dots, y_n)$ as the maximum chlorophyll measurement in a single year of n measurements. Over m years we have m yearly maxima, thus defining the observed annual maxima time series $x_1, x_2, \dots, x_m$. For an annual maximum x, the GEVD has a probability density function given by

$$p(x) = \frac{1}{\sigma} t(x)^{\xi+1} e^{-t(x)}$$

with

$$t(x) = \begin{cases} \left(1 + \xi\left(\frac{x-\mu}{\sigma}\right)\right)^{-\frac{1}{\xi}}, & \xi \neq 0, \\ e^{-\frac{x-\mu}{\sigma}}, & \xi = 0, \end{cases}$$

where μ, σ, and ξ are the location, scale, and shape parameters, respectively. The location parameter shifts the GEVD along the x axis, the scale parameter controls the spread, and the shape parameter controls the peaked-ness of the mode and heaviness of the distribution tail. Examples of how μ, σ, and ξ modulate the GEVD are given in **Figure 1**. Formulas for the expected value, variance, and mode of the GEVD are given in **Appendix A**.

In addition to the tree-parameter GEVD described above, we also apply a nonstationary extension where the parameters are described as simple linear functions of time (Gilleland and Katz 2016) of the form

$$\theta(t) = \theta_0 + \theta_1 t,$$

where θ is one of the GEVD parameters, θ_0 is the intercept of the linear relationship, and θ_1 is the slope, i.e. the rate of change with respect to time.

The log-likelihood for the GEVD parameters (Gilleland and Katz 2016) is given by

$$l(\mu, \sigma, \xi | x_1, x_2, \ldots, x_m) = -m \ln \sigma - \left(1 + \tfrac{1}{\xi}\right) \sum_{i=1}^{m} \ln\left(1 + \xi\left(\tfrac{x_i - \mu}{\sigma}\right)\right) - \sum_{i=1}^{m} \left(1 + \xi\left(\tfrac{x_i - \mu}{\sigma}\right)\right)^{1/\xi}.$$

We maximized the log-likelihood function with respect to the parameters to obtain empirical estimates. We maximized with respect to μ, σ, and ξ in the case of stationary GEVDs, and with respect to the intercept and slope in the case of nonstationary GEVDs. We restricted the analysis to estimating one nonstationary parameter at a time due to data restrictions and weak identifiability when multiple parameters are allowed to vary with time. We only considered linear functions of time and suggest nonlinear functions for future work. We used numerical optimization routines implemented in the extRemes library within the R programming language (Gilleland and Katz 2016). We compared stationary and nonstationary fits according to the Bayesian Information Criterion (BIC), given by $\text{BIC} = -2l(\hat{\mu}, \hat{\sigma}, \hat{\xi}) - k \log n$, where $l(\hat{\mu}, \hat{\sigma}, \hat{\xi})$ is the maximized likelihood at empirical estimates $\hat{\mu}$, $\hat{\sigma}$, and $\hat{\xi}$. k is the number of parameters in the GEVD (three for stationary GEVDs, four for nonstationary GEVDs), and n is the number of yearly maxima used in the fit. A GEVD was fit to chlorophyll time series in each ¼° pixel. The parameters were mapped spatially and correlated with basin bathymetry. Parameter uncertainty was derived by taking the square-root of the inverse Hessian matrix evaluated at the maximum likelihood estimates.

Results

177
178 The distributions of annual chlorophyll showed excellent agreement with those predicted from
179 the GEVD (**Figure 2**). Across the Atlantic basin, observed distribution quantiles correlated with
180 those from the fitted GEVDs at $r = 0.97$ on the arithmetic scale (**Figure 2a**) and $r = 0.98$ on the
181 log scale (**Figure 2b**). The spatial distribution of the quantile-quantile correlation was also
182 consistent across the basin, with no apparent relationship with latitude or distance from the coast
183 (**Figure 2c**). The region of largest disagreement occurred off the southwest coast of Europe, yet
184 correlations were still above $r = 0.7$ and remained so across the basin.
185
186 When fitted GEVD parameters were mapped spatially we found that parameter magnitude
187 closely followed basin bathymetry (**Figures 3-4**). Location and shape parameters were
188 consistently elevated on the shelf (<700m depth; **Figure 3c,d**; **Figure 4a,c**) with magnitudes 2-3
189 fold higher than in waters deeper than 700m. This result demonstrated that interannual bloom
190 magnitude and the 'heaviness' of the underlying distribution tail were both elevated on the shelf.
191 This occurred on the eastern and western sides of the basin. Deeper slope waters off the coast of
192 Greenland also showed elevated location and shape parameters. The largest parameter
193 magnitudes were found in the shallow Baltic Sea (**Figure 3c,d**; **Figure 4a,c**). The scale
194 parameter showed a different pattern with bathymetry where parameter magnitude was only
195 slightly elevated in shelf waters but showed a step-change decrease in the deepest waters
196 (>4000m; **Figure 3c**; **Figure 4b**); however, we note the aerial distribution of shelf vs. deep water
197 is markedly different, with deep waters limited to the southern half of the basin around the Mid-
198 Atlantic ridge while shelf seas are widely distributed (**Figure 3a**). Parameter uncertainty weakly
199 correlated with parameter magnitude for location and shape parameters with no clear spatial
200 pattern (**Supplementary Figure 1**). Scale parameter uncertainty was elevated in deeper water
201 (**Supplementary Figure 1**). The area-weighted average of the parameter coefficients of variation
202 (the standard deviation of the parameter uncertainty divided by the fitted mean parameter) was
203 0.11, 0.38, 0.24 for location, scale, and shape parameters, meaning the 1σ uncertainty was 11%,
204 38%, and 24% of the mean, respectively (**Supplementary Figure 1**).
205
206 We quantified the correlation between fitted GEVDs parameters using linear relationships
207 (**Figure 4d-f**). Bivariate relationships between parameters were well described by a linear
208 intercept and positive slope. The strongest relationship was found between fitted location and
209 shape parameters, again reflecting that GEVD distributions increase in magnitude and heavy
210 tailed-ness with decreasing bathymetric depth. We visually characterized how the GEVD
211 changes from deep to shelf waters using the fitted linear relationships (**Figure g-h**), noting that
212 this characterization represents the basin-averaged relationships so may not necessarily be
213 representative of individual regions.
214
215 Using a nonstationary GEVD analysis, we found weak evidence for temporal trends in GEVD
216 parameters, despite significant trends in chlorophyll levels and sea surface temperature across the
217 North Atlantic (**Figure 5**). Nonstationary parameters were favored in 34.3%, 29.9%, and 36.3%
218 of basin area for location, scale, and shape parameters, respectively (**Figures 5a-c**). Importantly,
219 the strength of evidence for nonstationary parameters did not clearly correlate with trends in
220 chlorophyll (**Figure 5d**; except possibly on the east Greenland slope), nor sea surface
221 temperature (**Figure 5e**). The weakest evidence for nonstationary parameters was found in the
222 area with the strongest sea surface temperature trends, specifically the warming-cooling dipole

pattern on the western side of the basin caused in-part by a slowdown of the Atlantic overturning circulation and associated northward heat transport (i.e. the North Atlantic 'warming hole'; Keil et al. 2020).

We repeated the GEVD parameter estimation using the OC-CCI chlorophyll product and found consistent results to those based on MODIS observations presented above. Quantile-quantile correlations showed a similarly good fit between observed OC-CCI quantiles and those predicted from the fitted GEVDs with a correlation of $r = 0.98$ in arithmetic space and $r = 0.98$ in log space (**Supplementary Figure 2**). Spatial patterns in fitted GEVD parameters were consistent across parameter sets estimated using the two datasets, despite some evidence for slightly reduced scale parameter magnitudes using OC-CCI chlorophyll (**Supplementary Figure 3**), which may be due to reduced variance in the synthetic multi-sensor OC-CCI dataset.

Discussion

Our analysis demonstrates that annual chlorophyll maxima are well-described by the GEVD based on the statistical theory of extreme values. We achieved a high goodness-of-fit and interpretable spatial patterns across the North Atlantic basin. A clear pattern emerged in the correlation between GEVD parameters and bathymetric depth, with the magnitude and tailed-ness of chlorophyll extremes increasing in shelf and slope environments. While the mechanism for this pattern will require further research, we hypothesize that nutrient and stratification dynamics may play a role. For example, elevated blooms are seen in other shelf and slope ecosystems related to nutrient delivery and water column stability controlled by the shelf-break circulation (Garcia et al. 2008). The heavy distribution tail on the shelf may also be related to variability in bloom timing which has been shown to impact interannual variability in shelf bloom magnitude (Friedland et al. 2015). We suggest further work examining the potential mechanisms that could explain different extreme value distributions under contrasting oceanographic environments. Classical models of phytoplankton blooms (e.g. Behrenfeld and Boss 2014) may be extended to include stochastic forcing and generate statistical distributions of bloom interannual magnitude. Targeted sensitivity of annual maxima distributions to different underlying forcing may uncover mechanisms for changes in distribution parameters across the shelf and open ocean.

Results of the nonstationary analysis suggested surprisingly weak evidence for changes in GEVD parameters over time. The lack of correlation with observed trends in background chlorophyll and sea surface temperature suggests that climate-related drivers are playing a limited role in modulating interannual bloom magnitude, despite the North Atlantic showing significant climate change (Keil et al. 2020). We note, however, that the current nonstationary analysis is limited by time series length. Continued studies will be required to monitor changes in bloom magnitude over time. An extended satellite record will provide greater statistical power to detect climate-driven trends. An extended record will also constrain more complicated functions describing the variation of parameters with time and their statistical association with environmental factors.

Ecologically, interesting questions arise about how extreme blooms propagate through food webs, contribute to carbon export, and impact ecological processes more broadly. For example, annual fisheries recruitment is often characterized by heavy-tailed distributions where individual

years exhibit extremely large cohorts, often fueling the fishery for years (Saetre et al. 2002). Extreme bloom years may increase the probability of strong cohorts via the match-mismatch mechanism (Platt et al. 2003), perhaps with temporal lags between blooms and recruitment modulated by trophic transfer. With respect to carbon export, we expect extreme blooms to contribute disproportionately to interannual carbon fluxes due to the commonly-observed positive effect of phytoplankton productivity on carbon export efficiency (Britten and Primeau 2016) and observed carbon fluxes associated with blooms in the North Atlantic (Briggs et al. 2011). Databases of carbon flux observations may be used to test this hypothesis at the basin scale (Mouw et al. 2016). Beyond fisheries and carbon export, we envision extreme event distributions to be broadly useful in characterizing the response of ecological processes to environmental extremes. The increase in applications of extreme value theory to environmental processes (Aghakouchak et al. 2020) naturally leads to questions of how environmental extremes impact ecology. The GEVD is one extreme value analysis tool that utilizes the distribution of block maxima (which was particularly appropriate here to describe the maxima of a repeating annual cycle) however other statistical descriptions of ecological heavy tailed-ness can also be useful in this context (e.g. Anderson et al. 2017).

In summary, the GEVD provided a useful statistical description of bloom variability and a general framework to quantify the spatiotemporal statistics of interannual bloom maxima. We hope this study spurns further analysis of marine ecosystem variability using extreme value theory to better understand how environmental conditions give rise to ecological extreme events, how extreme blooms contribute to fisheries productivity and carbon export, and how these processes may change with climate.

Acknowledgements

We gratefully acknowledge funding through the Simons Foundation Collaboration on Computational Biogeochemical Modeling of Marine Ecosystems and the Simons Foundation Postdoctoral Fellowship in Marine Microbial Ecology.

Data and Code Availability: All data used in this study are publicly available via the links given in the text. Code used to perform the GEVD analysis and visualize the results is publicly available at: https://github.com/gregbritten/chl_extremes_public.

References

Aghakouchak, A., F. Chiang, L. S. Huning, and others. 2020. Climate extremes and compound hazards in a warming world. Annu. Rev. Earth Planet. Sci. **48**: 519–548.

Anderson, S. C., T. A. Branch, A. B. Cooper, and N. K. Dulvy. 2017. Black-swan events in animal populations. Proc. Natl. Acad. Sci. **114**: 3252–3257.

Batt, R. D., S. R. Carpenter, and A. R. Ives. 2017. Extreme events in lake ecosystem time series. Limnol. Oceanogr. Lett. **2**: 63–69.

Behrenfeld, M. J. 2010. Abandoning sverdrup's critical depth hypothesis on phytoplankton blooms. Ecology **91**: 977–989.

Behrenfeld, M. J., and E. S. Boss. 2014. Resurrecting the ecological underpinnings of ocean plankton blooms. Ann. Rev. Mar. Sci. **6**: 167–194.

315 Behrenfeld, M. J., and E. S. Boss. 2018. Student's tutorial on bloom hypotheses in the context of
316 phytoplankton annual cycles. Glob. Chang. Biol. **24**: 55–77.
317 Briggs, N., M. J. Perry, I. Cetinić, C. Lee, E. D'Asaro, A. M. Gray, and E. Rehm. 2011. High-
318 resolution observations of aggregate flux during a sub-polar North Atlantic spring bloom.
319 Deep. Res. Part I Oceanogr. Res. Pap. **58**: 1031–1039.
320 Britten, G., and F. Primeau. 2016. Biome-specific scaling of ocean productivity, temperature,
321 and carbon export efficiency. Geophys. Res. Lett. **43**: 5210–5216.
322 Coles, S. 2001. An introduction to statistical modeling of extreme values, Springer-Verlag.
323 Dutkiewicz, S., M. Follows, J. Marshall, and W. W. Gregg. 2001. Interannual variability of
324 phytoplankton abundances in the North Atlantic. Deep. Res. Part II Top. Stud. Oceanogr.
325 **48**: 2323–2344.
326 Easterling, D. R., G. A. Meehl, C. Parmesan, S. A. Changnon, T. R. Karl, and L. O. Mearns.
327 2000. Climate extremes: observations, modeling, and impacts. Science **289**: 2068–2075.
328 Evans, G. T., J. S. Parslow, G. T. Evans, and J. S. Parslow. 1985. A model of annual plankton
329 cycles. Deep Sea Res. Part B. Oceanogr. Lit. Rev. **32**: 759.
330 Falkowski, P., R. Barber, and V. Smetacek. 1998. Biogeochemical controls and feedbacks on
331 ocean primary production. Science **281**: 200–206.
332 Falkowski, P., E. Laws, R. Barber, and J. Murray. 2003. Phytoplankton and their role in primary,
333 new and export production, p. 99–121. *In* M.J.R. Fasham [ed.], Ocean Biogeochemistry.
334 Springer.
335 Ferrari, R., S. T. Merrifield, and J. R. Taylor. 2015. Shutdown of convection triggers increase of
336 surface chlorophyll. J. Mar. Syst. **147**: 116–122.
337 Follows, M., and S. Dutkiewicz. 2002. Meteorological modulation of the North Atlantic spring
338 bloom. Deep Sea Res. Part II Top. Stud. Oceanogr. **49**: 321–344.
339 Friedland, K. D., R. T. Leaf, J. Kane, and others. 2015. Spring bloom dynamics and zooplankton
340 biomass response on the US Northeast Continental Shelf. Cont. Shelf Res. **102**: 47–61.
341 Garcia, V. M. T., C. A. E. Garcia, M. M. Mata, R. C. Pollery, A. R. Piola, S. R. Signorini, C. R.
342 McClain, and M. D. Iglesias-Rodriguez. 2008. Environmental factors controlling the
343 phytoplankton blooms at the Patagonia shelf-break in spring. Deep. Res. Part I Oceanogr.
344 Res. Pap. **55**: 1150–1166.
345 Gilleland, E., and R. W. Katz. 2016. extRemes 2.0: An extreme value analysis package in R. J.
346 Stat. Softw. **72**: 1–39.
347 Ito, T., and M. J. Follows. 2005. Preformed phosphate, soft tissue pump and atmospheric CO2. J.
348 Mar. Res. **63**: 813–839.
349 Katz, R. W. 2010. Statistics of extremes in climate change. Clim. Change **100**: 71–76.
350 Keil, P., T. Mauritsen, J. Jungclaus, C. Hedemann, D. Olonscheck, and R. Ghosh. 2020. Multiple
351 drivers of the North Atlantic warming hole. Nat. Clim. Chang. **10**: 667–671.
352 Maritorena, S., and D. a. Siegel. 2005. Consistent merging of satellite ocean color data sets using
353 a bio-optical model. Remote Sens. Environ. **94**: 429–440.
354 Mouw, C. B., A. Barnett, G. A. Mckinley, L. Gloege, and D. Pilcher. 2016. Global ocean
355 particulate organic carbon flux merged with satellite parameters. Earth Syst. Sci. Data **8**:
356 531–541.
357 Platt, T., C. Fuentes-Yaco, and K. T. Frank. 2003. Spring algal bloom and larval fish survival.
358 Nature **423**: 398–399.
359 Saetre, R., R. Toresen, and T. Anker-Nilssen. 2002. Factors affecting the recruitment variability
360 of the Norwegian spring-spawning herring (Clupea harengus L.). ICES J. Mar. Sci. **59**:

725–736.
Sathyendranath, S., R. J. W. Brewin, C. Brockmann, and others. 2019. An ocean-colour time series for use in climate studies: The experience of the ocean-colour climate change initiative (OC-CCI). Sensors **19**: 1–31.
Siegel, D. A., S. C. Doney, and J. A. Yoder. 2002. The North Atlantic spring phytoplankton bloom and Sverdrup's critical depth hypothesis. Science **296**: 730–733.
Sommer, U., and K. Lengfellner. 2008. Climate change and the timing, magnitude, and composition of the phytoplankton spring bloom. Glob. Chang. Biol. **14**: 1199–1208.
Taylor, J. R., and R. Ferrari. 2011. Ocean fronts trigger high latitude phytoplankton blooms. Geophys. Res. Lett. **38**: 1–5.
Visser, F., K. L. Hartman, G. J. Pierce, V. D. Valavanis, and J. Huisman. 2011. Timing of migratory baleen whales at the azores in relation to the north atlantic spring bloom. Mar. Ecol. Prog. Ser. **440**: 267–279.

Figures

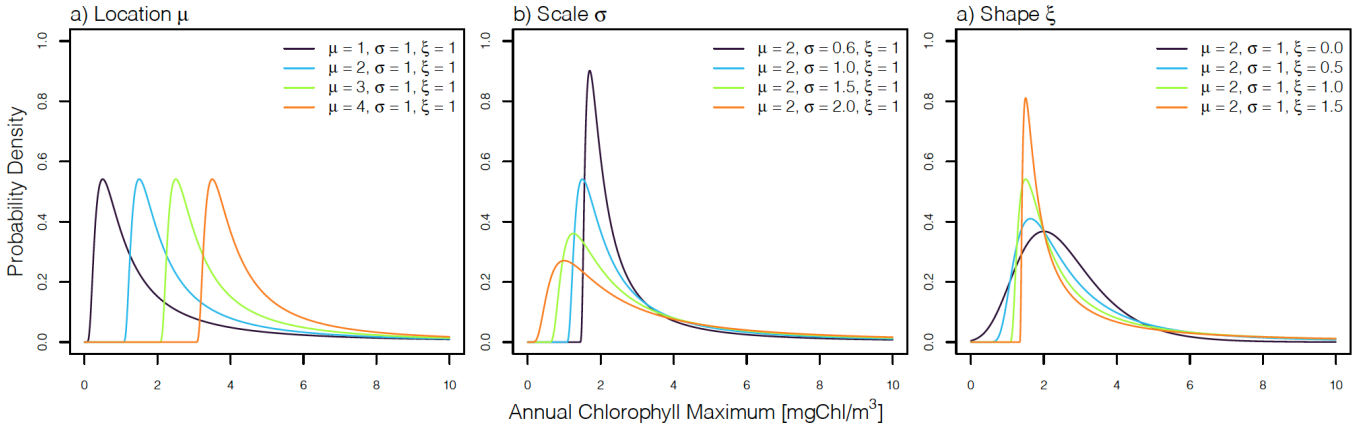

Figure 1. Examples of the GEVD distribution for different values of the location (**a**), scale (**b**), and shape (**c**) parameters.

381

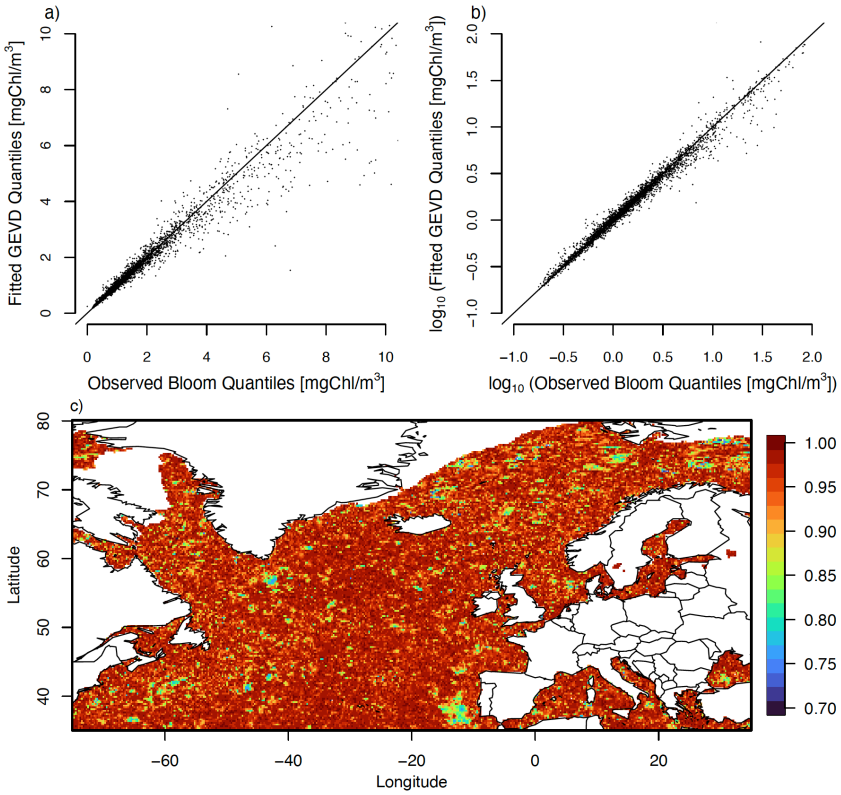

382
383

384 Figure 2. Observed quantiles of North Atlantic annual bloom extremes vs. those predicted from
385 the fitted GEVDs. Panel **a** gives the relationship in arithmetic space; panel **b** gives the
386 relationship in log (base ten) space. A random sample of 5000 quantiles were drawn in order to
387 visualize the relationship in **a** and **b**. The correlations in **a** and **b** are 0.97 and 0.98, respectively.
388 Panel **c** gives the spatial distribution of quantile-quantile correlations. Note the correlation color
389 bar extends from 0.7 to 1.0.

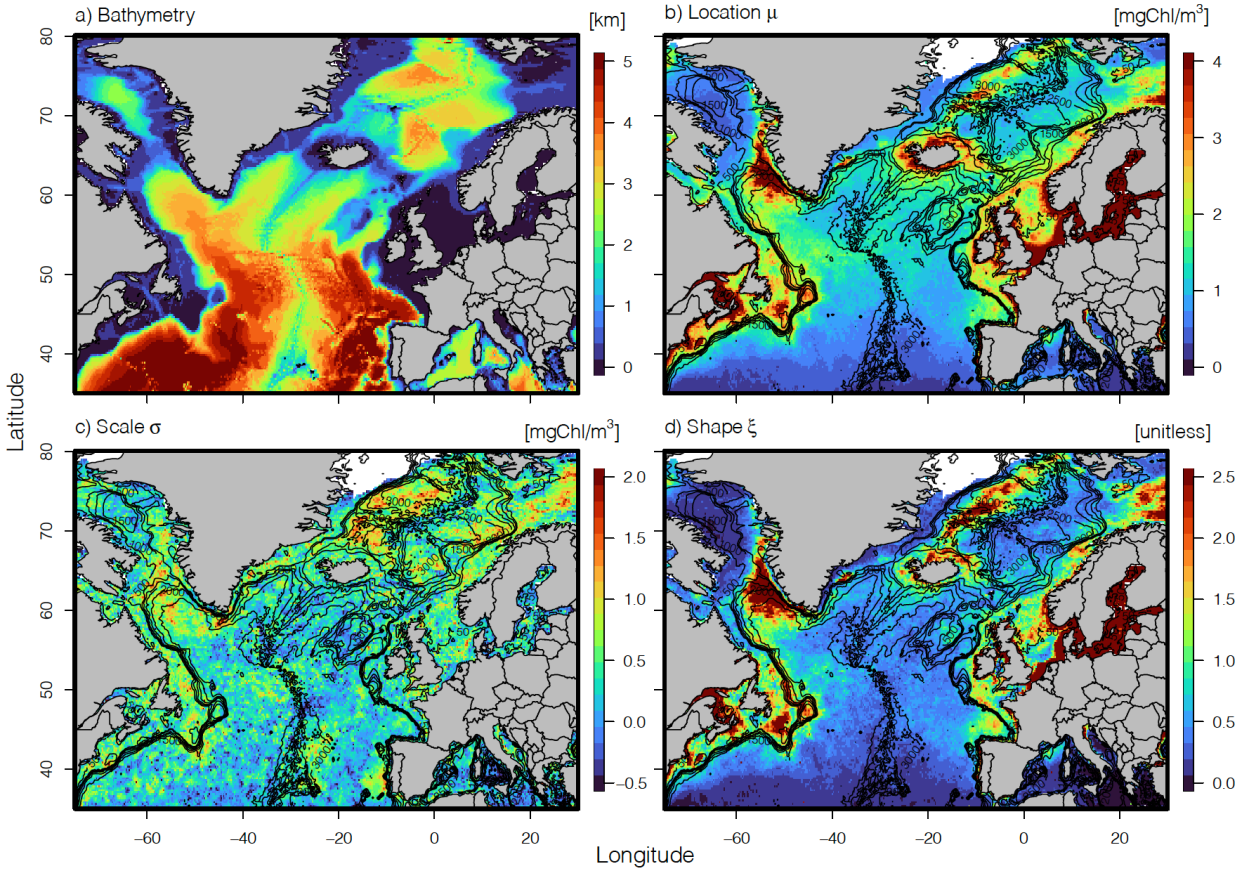

Figure 3. Spatial distribution of fitted GEVD parameters and basin bathymetry. Panel **a** gives the bathymetric depth in the North Atlantic basin. Panels **b**, **c**, and **d** give the estimated location, scale, and shape parameters, respectively. Bathymetry contours are overlaid in **b**-**d** with a contour interval of 500 meters.

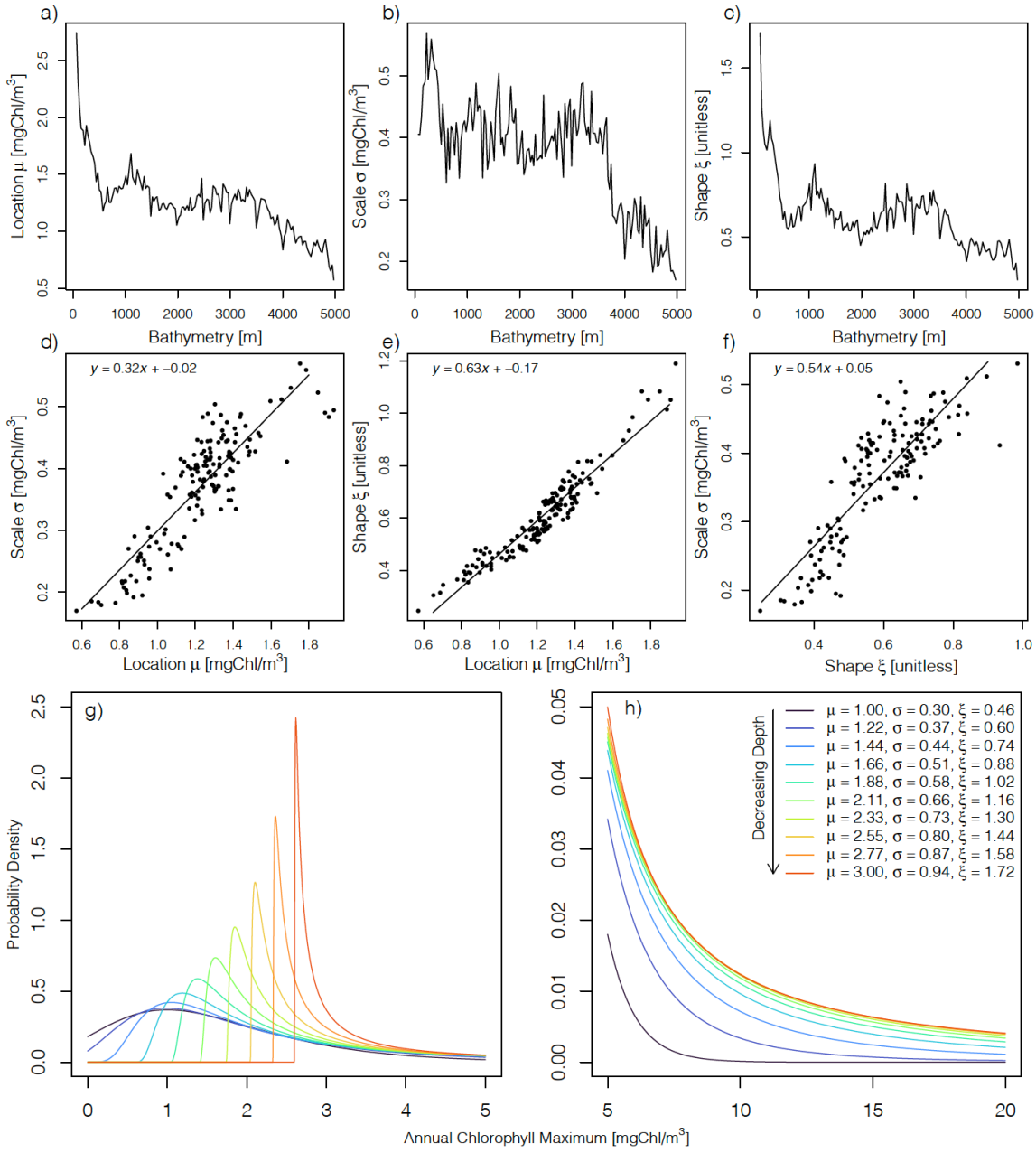

Figure 4. Relationships between fitted GEVD parameter and bathymetric depth. Panels **a**-**c** give the basin-averaged relationship between the fitted parameters and bathymetric depth. Panels **d**-**f** give the inter-relationships among fitted parameters with the least squares regression line and equation. Panels **g** and **h** give the basin-averaged change of the GEVD with bathymetric depth. Panel **h** zooms in on the distribution tail in **g** (note horizontal axis limits).

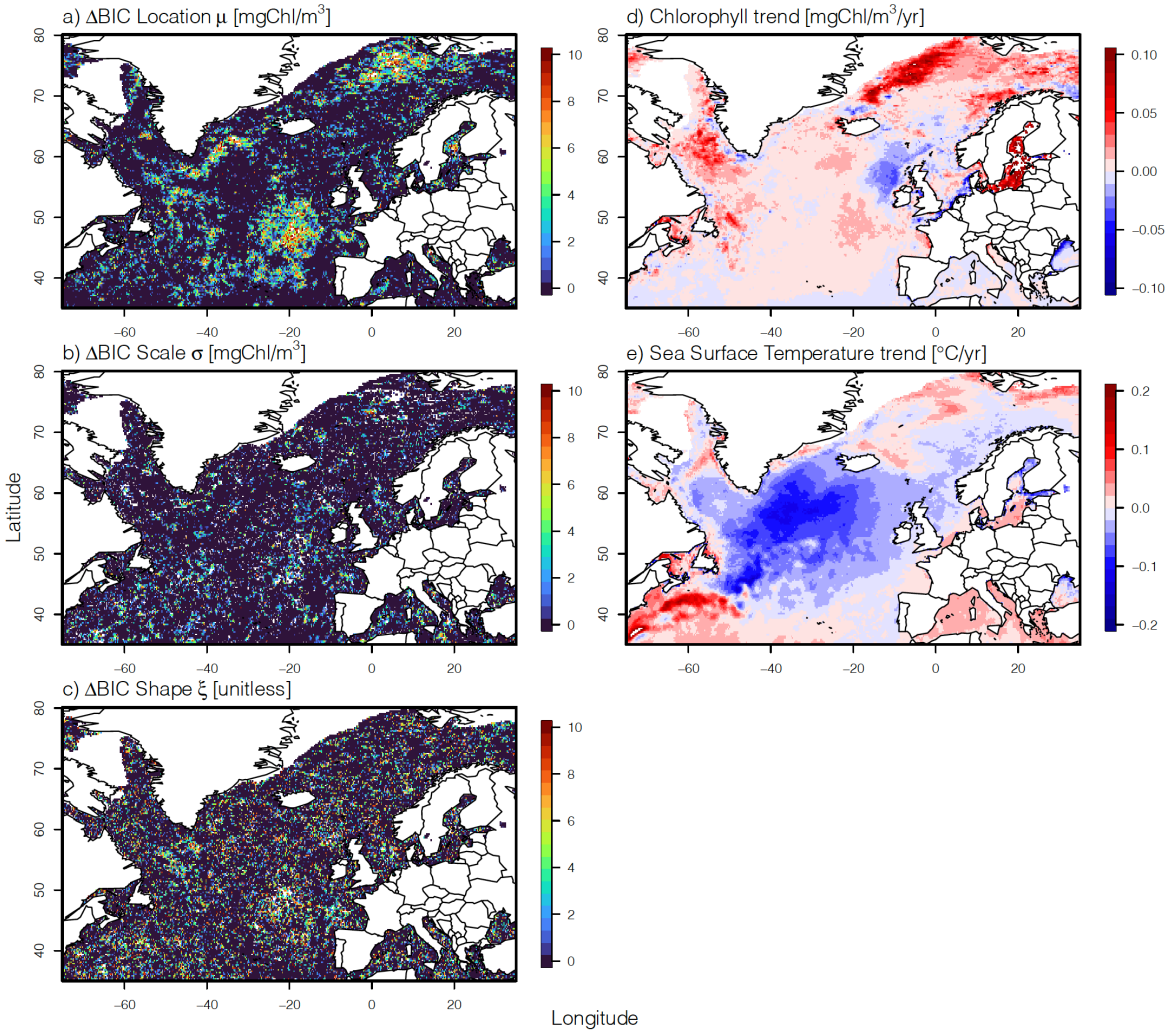

Figure 5. Evidence for nonstationary GEVD parameters in the context of basin-scale trends in chlorophyll and sea surface temperature. Model selection results comparing stationary and nonstationary GEVDs using the Bayesian Information (BIC) are given in panel **a** (nonstationary location parameter), **b** (nonstationary scale), and **c** (nonstationary shape). The difference in BIC (ΔBIC) is given relative to the stationary model. Non-zero values indicate the nonstationary model is favoured and the magnitude indicates the relative strength of evidence. Panels **d** and **e** give the linear trend in surface chlorophyll and sea surface temperature, respectively, estimated from MODIS observations since 2002.

Appendix A

The expected value of the GEVD is given by

$$\mathbf{E}[x] = \begin{cases} \mu + (g(1) - 1)\dfrac{\sigma}{\xi} & if\ \xi \neq 0, \xi < 1 \\ \mu + \sigma\gamma & if\ \xi = 0 \\ \infty & if\ \xi > 1 \end{cases}$$

where $g(k) = \Gamma(1 - k\xi)$, $\Gamma(r)$ is the gamma function, and γ is Euler's constant ($\gamma \cong 0.5772$). The variance of the GEVD is

$$\mathbf{Var}[x] = (g(2) - g(1)^2)\frac{\sigma^2}{\xi^2}.$$

The mode of the GEVD is

$$\mathbf{Mode}[x] = \mu + \frac{\sigma}{\xi}((1 + \xi)^{-\xi} - 1).$$

Supplemental Information:

Extreme value distributions describe interannual variability in the North Atlantic spring bloom

Gregory L. Britten
Program in Atmospheres, Oceans, and Climate
Massachusetts Institute of Technology, Cambridge, MA, USA
gregleebritten@gmail.com

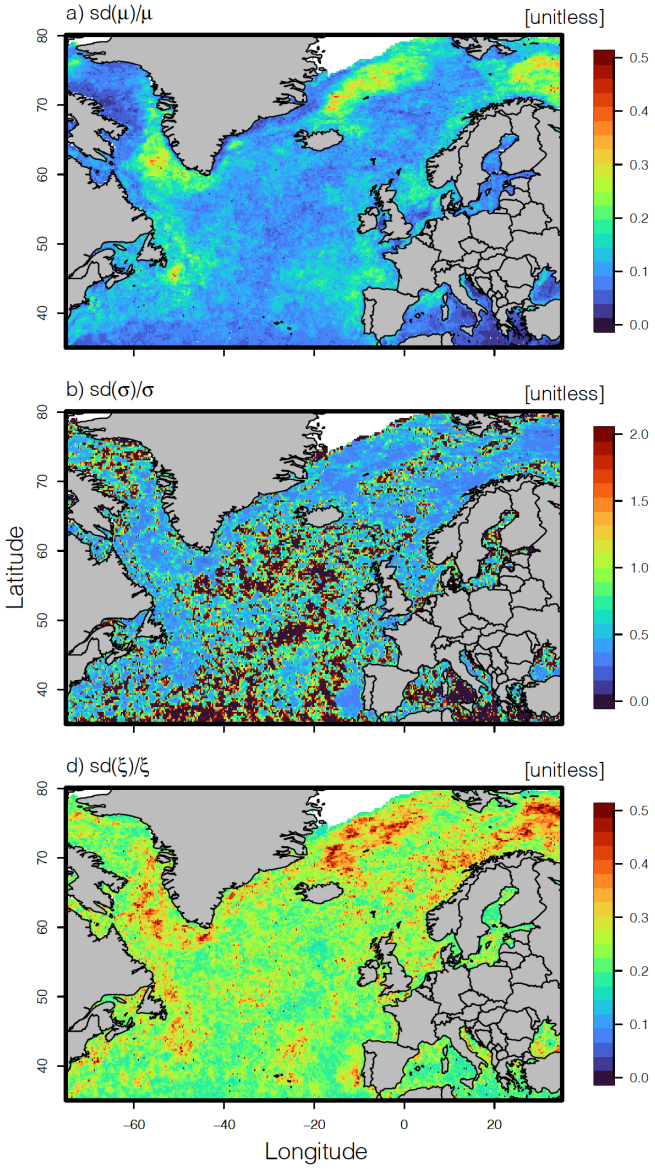

Supplementary Figure 1. Uncertainty in fitted GEVD parameters expressed as the coefficient of variation (CV). The CV is calculated as the ratio of the uncertainty standard deviation divided by the mean of the fitted parameter.

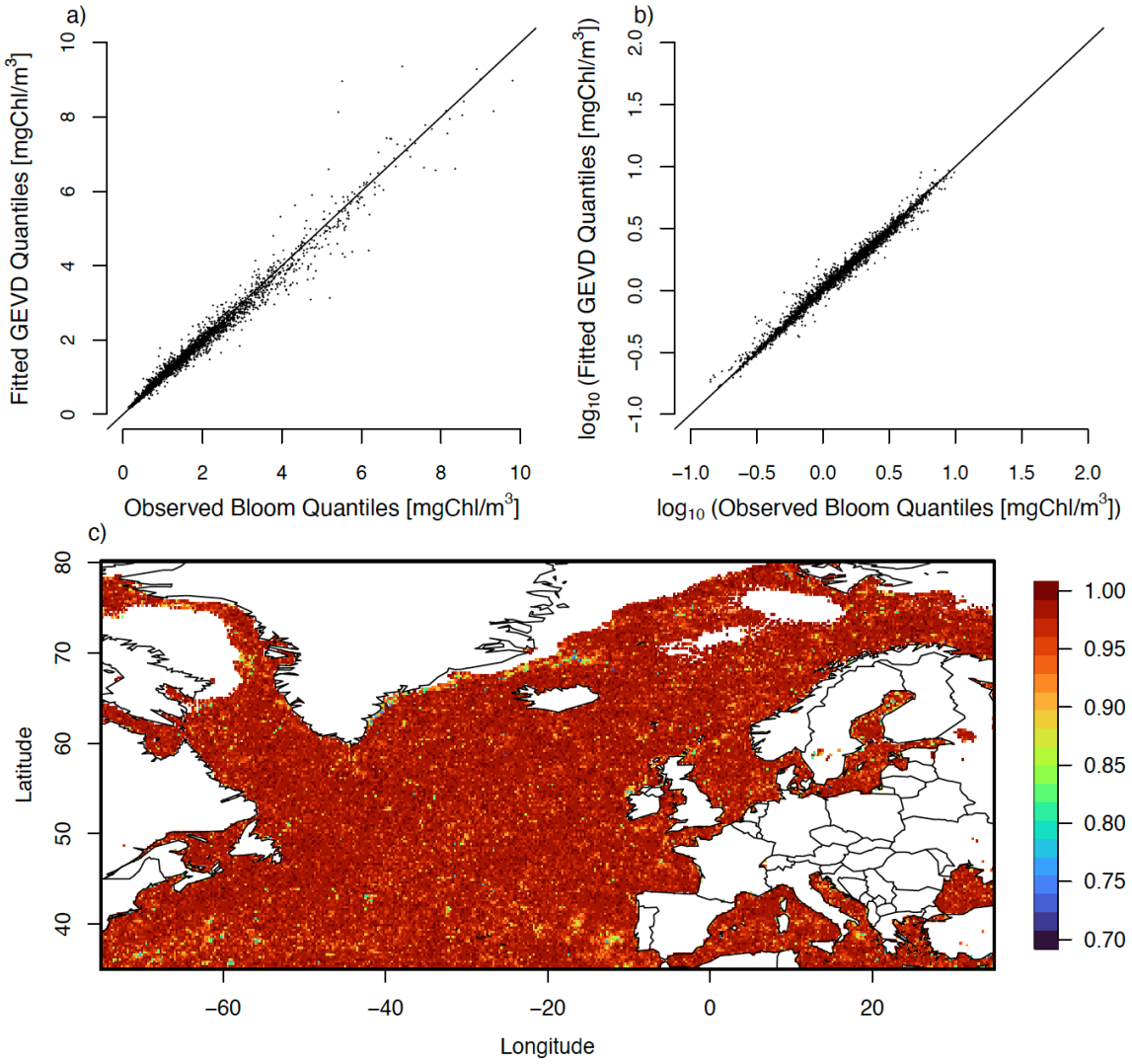

Supplementary Figure 2. As in Figure 2 of the main text but using OC-CCI chlorophyll estimates

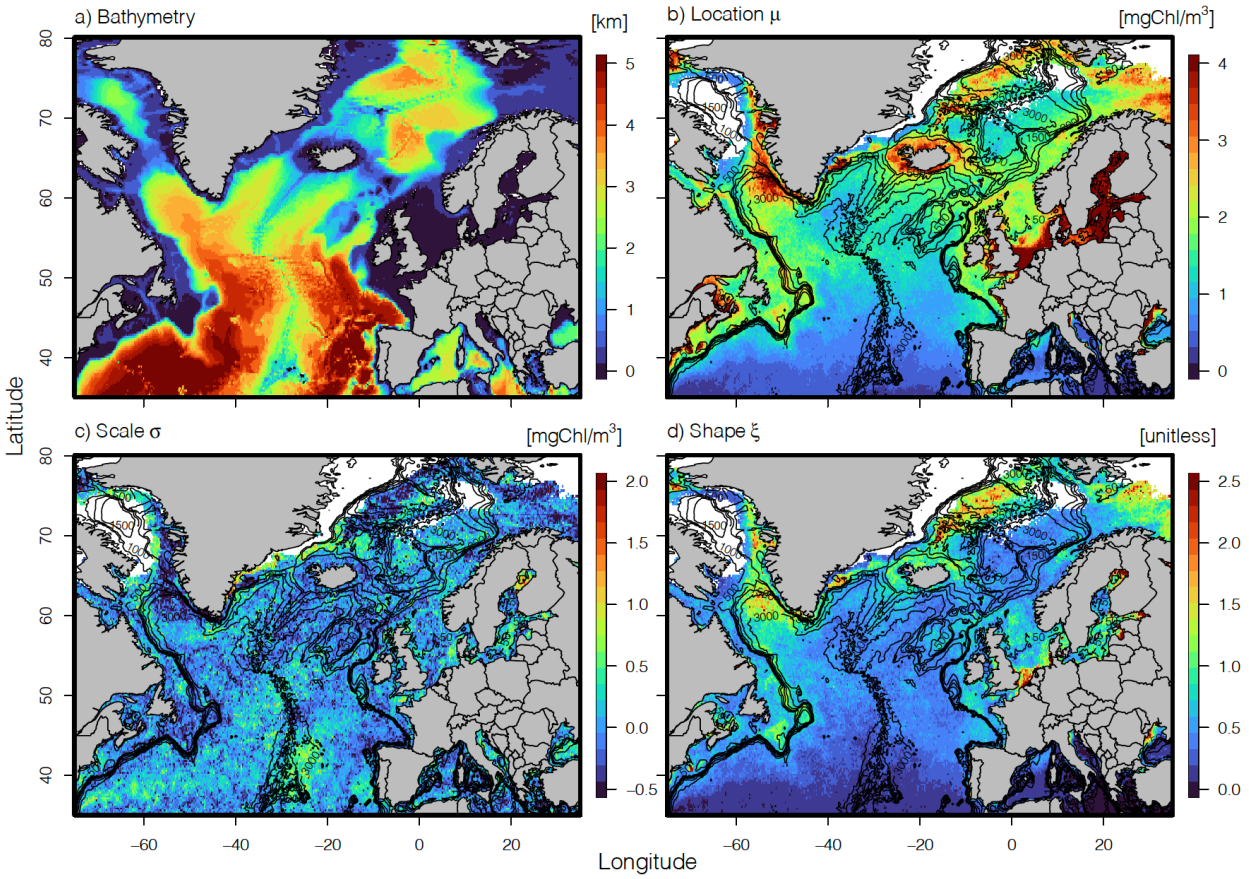

Supplementary Figure 3. As in Figure 3 of the main text but using OC-CCI chlorophyll estimates.